Environmental Technology & Innovation 31 (2023) 103229

Contents lists available at ScienceDirect

Environmental Technology & Innovation

journal homepage: www.elsevier.com/locate/eti

Modeling biochar-soil depth dependency on fecal coliform straining under subsurface drip irrigation

Forough Abbasi Teshnizi [a], Mahdi Ghobadinia [a], Fariborz Abbasi [b], Paul D. Hallett [c], Nasrollah Sepehrnia [c,*]

[a] Department of Water Engineering, Faculty of Agriculture, Shahrekord University, Shahrekord, Iran
[b] Agricultural Engineering Research Institute (AERI), Agricultural Research, Education and Extension Organization (AREEO), Karaj, Iran
[c] School of Biological Sciences, Cruickshank Building, St Machar Drive, Aberdeen, AB24 3UU, Scotland, United Kingdom

ARTICLE INFO

Article history:
Received 22 December 2022
Received in revised form 28 April 2023
Accepted 27 May 2023
Available online 2 June 2023

Keywords:
Biochar
Irrigation strategy
Soil bacteria contamination
Maximum allowable depletion
HYDRUS
Mathematical modeling

ABSTRACT

Biochar has several benefits for soil, including improved flow and retention properties that decrease bacterial transport. To improve understanding of the underlying mechanisms and optimal irrigation strategies for contaminated gray water, we conducted a lysimeter study exploring impacts of biochar level (0, 0.5, and 1% w/w) and 30-days irrigation regime (0.003 and 0.0064 cm h^{-1}). Biochar did not change hydraulic properties but at maximum allowable depletion (MAD) of 30, 50, and 70% biochar had a large impact on fecal coliform retention. At 15–25 cm depth where the subsurface dripper was located, 1% biochar-treated soil had 1.5 times greater retention than the controls. A combination of the lower irrigation rate (0.003 vs. 0.0064 cm h^{-1}) and the greater biochar (1% vs. 0.5%) had greater impacts on bacteria inactivation and retention than the MAD levels. Nevertheless, adding 1% biochar resulted in a 2-fold increase of bacteria retention for 30% MAD and low flow rate than greater flow rates and MAD levels (50 and 70%). Our results provided novel data for inverse optimization to explore bacteria retention by differences in bacteria attachment, straining, survival or growth. Close to the irrigation dripper, straining was the pronounced mechanism under the best performing treatment of 1% biochar and 30% MAD. Therefore, we recommend application of biochar at the rate of 1% where wastewater is used for subsurface drip irrigation.

1. Introduction

Biochar is widely applied in soil and studies show that its characteristics not only affect soil physicochemical properties and biological activities, but also control microbial contamination (Mohanty et al., 2014). This occurs because the chemical properties of biochar, such as volatile organic matter (OM) content, polarity (Valenca et al., 2021), cations (Rivera-Utrilla et al., 2001; Suliman et al., 2017), ash content, carbon content (Valenca et al., 2021), pH (Bolster and Abit, 2012; Thies and Rillig, 2012), solution ionic strength, and cation exchange capacity (CEC) (Zhu et al., 2017) can impact bacteria transport and retention. Bolster and Abit (2012) reported that the increase of bacterial deposition after adding biochar to soil was due to an increase in ionic strength, which decreases the thickness of the electrical double layer around the bacteria and soil particles. An increase of cations (*e.g.*, Ca^{2+}, Mg^{2+}, Na^{+} and K^{+}) in soil from biochar amendment can also result

* Corresponding author.
E-mail address: nasrollah.sepehrnia@abdn.ac.uk (N. Sepehrnia).

https://doi.org/10.1016/j.eti.2023.103229

List of symbols, acronyms and units

Parameter	Definition (Unit)
q	Discharge rate equal to 0.003 (cm h^{-1})
Q	Discharge rate equal to 0.0064 (cm h^{-1})
MAD	Maximum Allowable Depletion/ Management Allowed Depletion (%)
k_{att}	Attachment coefficient (h^{-1})
k_{det}	Physical detachment coefficient (h^{-1})
k_{str}	Straining coefficient (h^{-1})
μ_l	Inactivation coefficient in liquid phase (h^{-1})
μ_s	Inactivation coefficient in solid phase (h^{-1})
θ_v	Volumetric soil moisture content (cm^3 cm^{-3})
θ_{fc}	Soil water content at field capacity (cm^3 cm^{-3})
θ_{pwp}	Soil water content at permanent wilting point (cm^3 cm^{-3})

in linking metal cations to the outer membrane of bacteria, further enhancing bacteria retention (Suliman et al., 2017; Rivera-Utrilla et al., 2001). Valenca et al. (2021) found that bacteria removal was negatively correlated with ash content, and polar and volatile OM content. Further, physical properties of biochar impact bacteria transport and retention, such as surface area, hydrophobicity, particle size and pore size (Lehmann et al., 2011; Mohanty and Boehm, 2014).

Of these physical properties, the high surface area of biochar (1 to 100 m^2 g^{-1}) likely has the most marked impact on bacteria retention (Thies and Rillig, 2012). Since surface area is related to biochar size, Mohanty and Boehm (2014) found that *E. coli* retention in sand columns was more effective for small (<125 μm) rather than large particles of biochar. Moreover, changes in water content of porous media can alter biochar hydrophobicity and this may be responsible for changes in bacteria retention (Abit et al., 2014). Biochar with its small bulk density (0.08 to 0.7 g cm^{-3}) compared to soil (Abel et al., 2013) can also affect porosity (Das and Ghosh, 2022; He et al., 2021; Toková et al., 2020), leading to greater retention of bacteria (Yin et al., 2021).

The pores of biochar have a size distribution affected by the feedstock and pyrolysis, so scope exists to produce biochar with greater potential for bacteria retention (Perez-Mercadoa et al., 2019; Vieira et al., 2021). Biochar pores can be classified into three size categories based on diameter: micropores (<2 nm), mesopores (2–50 nm), and macropores (>50 nm) (Guo et al., 2021; Ponnusamy et al., 2020). If bacteria are larger than the pore size, then straining will be the physical mechanism, whereas if the bacteria are smaller than the pore size, then attachment is the physcio-chemical mechanism of bacteria retention. Attachment of bacteria occurs more commonly and is usually effective when biochar pore sizes are 2 to 5 times larger than the bacteria cell size (Lehmann et al., 2011), so dominated by macropores (Aller, 2016).

Although biochar effects on bacteria transport and retention through porous media have been studied extensively (Gurtler et al., 2014; Kaetzl et al., 2019; Sasidharan et al., 2016), the research has been limited to column studies or biofilters. Under more realistic conditions of subsurface drip irrigation systems at field or lysimeter scale, little information is available. Cui et al. (2019) reported that soil mixed with biochar (1% w/w) compared to an unamended control had a significant increase in the abundance of pathogenic bacteria in soil after a 60-day cultivation of maize in a rhizobox that was irrigated with reclaimed water and pig wastewater. Arief Ismail et al. (2016) demonstrated that mixing 1% biochar in the top 10 cm of soil combined with poultry manure increased pathogenic bacteria retention and limited bacteria transport through depth soil over a 60 days rainfall experiment.

Clearly the fate and wider environmental transport of bacteria in soil is affected by biochar amendment, but the small amount of available data limits the capacity to make predictions. Much more could be understood about retention and transport mechanisms using modeling, such as HYDRUS–2D/3D. Various lysimeter and field-based studies have applied HYDRUS–2D/3D to explore these processes, but not yet on biochar amended soils. An example is Amin et al. (2014) who applied HYDRUS–2D to simulate the redistribution and persistence of slurry-borne contaminants through soil following a direct injection of slurry over a 50-day period. They found that HYDRUS predicted accurately *E. coli* concentrations spatially and temporally using a two-site attachment–detachment model, but at high retention the predictions could be either overestimated or underestimated. Another HYDRUS study Morales et al. (2015), exploring a conventional soil-based wastewater treatment system, found bacteria die-off rates and the attachment/detachment variables were the main mechanisms. By modeling they were able to simulate the effects of hydraulic load rates, bacteria concentration, and precipitation pattern changes on bacteria transport.

The fate and retention of bacteria emitted from irrigation drippers during wastewater irrigation have also been modeled with HYDRUS–2D/3D. Akhavan et al. (2018) used HYDRUS–2D to evaluate the transport of *E. coli* through preferential flow in artificial macropores in saturated soil columns. They found that the model accurately predicted bacteria concentration in the soil matrix and macropores using the two kinetic attachment–detachment model. However, another study simulating

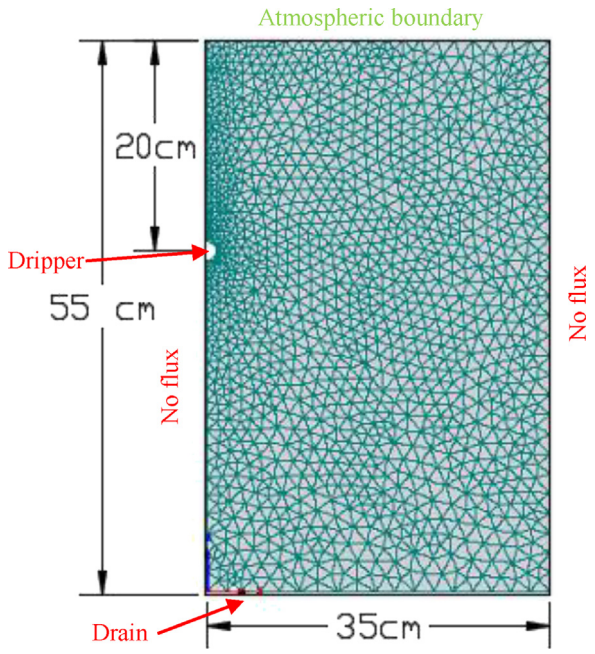

Fig. 1. A schematic view of the finite element mesh with boundary conditions based on the experimental layout, dripper and drain locations.

E. coli distribution from drip irrigation with sewage effluents using filtration theory and a two kinetic sites model by HYDRUS–2D/3D showed filtration theory was not useful for real bacteria transport (Wen et al., 2017).

Scope therefore exists to extend HYDRUS–2D/3D to predict transport and retention mechanisms of bacteria in biochar-amended soils irrigated with contaminated wastewater. Such understanding would give confidence to the use of biochar as a soil amendment in such systems. From recent data, maximum bacteria retention occurred at depths close to dripper, particularly at rate of 1% biochar (Teshnizi et al., 2023). In this study we explore these processes further in a lysimeter study, providing novel data to assess retention mechanisms and test HYDRUS–2D more thoroughly. Our main objective was to determine how biochar application rate and irrigation strategies affected the dominant retention mechanisms of bacteria. This has practical applications to illustrate the impacts of biochar in controlling bacterial pollution in agricultural soils in subsurface drip irrigation. We thus tested the following hypotheses; (i) the retention mechanism varies for the applied biochar rates, (ii) biochar retention efficiency depends on soil depth rather than the biochar application rate, and (iii) HYDRUS–2D can robustly determine bacteria retention mechanisms (Sepehrnia et al., 2019, 2018). The research used a well-controlled set of lysimeter experiments with agricultural soil to determine how biochar, irrigation discharge rates as well as irrigation management could affect soil hydraulic properties and bacteria transport and fate. Finally, water flow and bacteria transport were optimized for various soil depths using HYDRUS–2D.

2. Materials and methods

2.1. Lysimeter preparation and subsurface drip irrigation

Soil samples were taken from the research farm of the Shahrekord University, Agricultural College, Iran. The soil is classified as an Inceptisol (Soil Survey Staff, 2014) and was planted with Corn (*Zee mays*). It was sampled from the plough layer at 0 to 30 cm depth. The soil was air-dried and passed through a 2 mm sieve to remove large plant roots and stones. It was then mixed with a biochar at rates of 0, 0.5, and 1% w/w (Wang et al., 2019), roughly equivalent to concentrations that would occur at field application rates of 3 to 6.5 t ha^{-1}. The biochar had a particle diameter smaller than 2 mm and was produced commercially from soft wood materials of pomegranate (*Punica granatum*) and plum (*Prunus domestica*) that were pyrolyzed at 450–500 °C (Sun Company, Iran).

The sieved soils (with the initial water content equals to 0.09 ($\pm$0.01) cm^3 cm^{-3}) were packed into lysimeters (70 $\times$ 17 $\times$ 60 cm, L$\times$W$\times$D) made from glass. The walls of the lysimeters were treated with a very thin layer of grease prior filling in order to prevent preferential flow along the walls (Kandelous and Šimůnek, 2010a). The lysimeters were filled with the biochar-treated soil and without biochar as the controls. Bulk density of the lysimeters was equal to field density (1.3 g cm^{-3}).

For irrigation, a dripper was installed at a depth of 20 cm at the center of each lysimeter (Fig. 1) and connected to a reservoir filled with wastewater containing bacteria (3.99 $\pm$ 1.4 $\times$ 10^5 CFU ml^{-1}). Drainage was directed through two

Table 1
Soil hydraulic parameters used for the simulations.

Treatments	θ_r (cm^3 cm^{-3})	θ_s (cm^3 cm^{-3})	α (cm^{-1})	n (_)	K_s (cm h^{-1})	l (_)
Soil + 0% biochar	0.08	0.395	0.062	1.57	0.85	0.5
Soil + 0.5% biochar	0.08	0.399	0.064	1.53	0.86	0.5
Soil + 1% biochar	0.081	0.415	0.067	1.47	0.87	0.5

drains about 2 cm diameter at the bottom of the lysimeters to collect effluents. Irrigation was performed when the soil water content reached maximum allowable depletion (θ_{MAD}). The depth of irrigation water and the values of θ_{MAD} were calculated using Eqs. (1) and (2), respectively (Martin et al., 1990):

$$\theta_{MAD} = \theta_{FC} - (\theta_{FC} - \theta_{PWP}) \times MAD \quad (1)$$

$$d = (\theta_{FC} - \theta_{MAD}) \times D \quad (2)$$

where θ_{Fc} and θ_{PWP} are the volumetric water contents at field capacity (cm^3 cm^{-3}) and permanent wilting points (cm^3 cm^{-3}), respectively (see Section 2.2. for measurement approach). The MAD represents the maximum allowable depletion (%), D is the depth of the soil (cm), and d is the irrigation water depth (cm). In the first irrigation, all lysimeters were irrigated to field capacity (Forslund et al., 2011), but the second and third irrigations were performed according to the MAD related to either treatments. For this, soil water content was measured using a SM300 moisture meter (Delta-T Devices, UK) at the irrigation intervals by inserting the probe through small pores already installed on the right side of the lysimeters wall. These measurements were at 5, 17, and 29 cm from the dripper and 5, 15, 25, 35, and 45 cm depths below the soil surface. The three middle depths (i.e., 15, 25, 35 cm) were used to control irrigation rates to maintain the soil the field capacity. The lysimeters walls were protected from direct radiation of sunlight during the experiments by wrapping in opaque plastic sheeting.

2.2. Soil routine measurements

Soil texture was measured by sedimentation and a hydrometer (Gee and Bauder, 1986). An EC-meter measured electrical conductivity (EC) in soil solution (Rhoades, 1996; Sims, 1996). The specific surface areas of biochar and soil were determined by the Brunauer–Emmett–Teller (BET) method (Brunauer et al., 1938). The pH (1:5 soil:water) of soil was measured using a pH-meter (Rayment and Higginson, 1992). A pressure plate was used to determine the soil moisture retention curve at 0, 0.03, 0.1, 0.5, 1.0, and 1.5 MPa (Klute, 1986) of soil-biochar mixtures.

2.3. Bacteria

For bacteria preparation, fecal coliforms were harvested from raw wastewater provided by Shahrekord Wastewater Treatment Plant, Iran. MacConkey agar was used to grow cells at 44.5 °C for 24 h. This was then used to produce a bacteria suspension (30 ± 9.2 ml) containing $3.99 \pm 1.4 \times 10^5$ (CFU mL^{-1}) that was added to the irrigation water used throughout the experiment (Song et al., 2006). The influent concentration was always controlled using the plate counting method in triplicates prior of each irrigation.

Soil samples were collected from depths of 0–5, 15, 20, 25 and 50 cm to determine fecal coliform distribution through the lysimeter. At the installed dripper at depth 20 cm, the samples were taken from the final lateral margin of the wetting front, not directly parallel to the up or down dripper locations (Table 1, supplementary data). At each irrigation soil samples were taken before irrigation and at 0, 24 and 48 h after stoppage, and then immediately transferred to the lab. One gram of each of the soil samples, in three replications, was weighed and placed into containers with 9 ml of sterilized distilled water, and then mixed using a shaker for 30 min (Guber et al., 2005). A serial dilution (i.e., 1000–10000 times) was used to culture cells on MacConkey agar culture medium. The incubation was performed for 24 h at 44 ± 0.5 ° C. Finally, the number of bacteria colonies was counted from live cells by the plate count method and expressed as the colony forming units per ml (CFU mL^{-1}) of irrigation water (Guber et al., 2006).

2.4. Modeling

HYDRUS–2D simulated bacteria transport and water flow. This software package numerically solves the Richardson–Richards equation for variably saturated water flow as (Šimůnek et al., 2012):

$$\frac{\partial \theta}{\partial t} = \frac{\partial}{\partial x_i}\left\{K(h)\left(K_{ij}^A \frac{\partial h}{\partial x_j} + K_{iz}^A\right)\right\} - S \quad (3)$$

where θ is the volumetric soil water content (cm^3 cm^{-3}), t is time (h), h is the pressure head (cm), K is the unsaturated hydraulic conductivity (cm h^{-1}), K_{ij}^A is a component of a dimensionless anisotropy tensor K^A, x_i is the spatial horizontal and vertical coordinates (cm), and S is the sink term (cm^3 cm^{-3} h^{-1}).

HYDRUS–2D employs a modified form of the convection–dispersion equation to model transport and fate of virus, colloid, and bacteria, as (Šimůnek et al., 2012):

$$\frac{\partial \theta c}{\partial t} + \rho \frac{\partial s_e}{\partial t} + \rho \frac{\partial s_1}{\partial t} + \rho \frac{\partial s_2}{\partial t} = \frac{\partial}{\partial x_i}(\theta D_{ij}^{w} \frac{\partial c}{\partial x_j}) - (\frac{\partial q_i c}{\partial x_i}) - \mu_w \theta c - \mu_s \rho (s_e + s_1 + s_2) \quad (4)$$

where c is the concentration of bacteria in aqueous phase (CFU mL^{-1}), s is the concentration of bacteria in solid phase (CFU mL^{-1} g^{-1}) with subscripts e,$_1$, and$_2$ denote equilibrium and two kinetic sorption sites, respectively, ρ is the bulk density (g cm^{-3}), q is the specific discharge (cm^3 h^{-1}); D_{ij} is an effective dispersion coefficient tensor (cm^2 h^{-1}), and μ_w and μ_s represent degradation and inactivation processes in the liquid and solid phases, respectively. The longitudinal and transversal dispersivity coefficients in this study were initially set one-tenth of the simulation domain and one-tenth of longitudinal dispersivity, respectively (Elasbah et al., 2019), and refined with trial-and-error. Mass transfer between the aqueous and solid kinetic phases can be represented as (Šimůnek et al., 2012):

$$\rho \frac{\partial s}{\partial t} = \theta k_a \psi c - k_d \rho s \quad (5)$$

where k_a is the first order deposition coefficient (h^{-1}), k_d is the first order entrainment coefficient (h^{-1}), and Ψ is a dimensionless colloid retention function. Ψ can be described as (Šimůnek et al., 2012):

$$\psi = \frac{s_{\max} - s}{s_{\max}} \quad (6)$$

where s_{max} is the maximum solid phase concentration (CFU $mL^{-1}g^{-1}$). In Eq. (4), it is assumed that soil has two sorption sites, s_1 and s_2, each with their own attachment and detachment constants. Sorption sites s_1 and s_2, can be used to represent straining and attachment, respectively. Bradford et al. (2003) suggested a depth-dependent blocking coefficient for the straining process (Eq. (7)).

$$\psi = \left(\frac{d_c + z + z_0}{d_c} \right)^{-\beta} \quad (7)$$

where d_c is the diameter of the sand grains (cm), z_0 is the location where straining starts (cm), and β is an empirical factor. Bacteria attachment and straining were evaluated using a two kinetics site model (Amin et al., 2014).

2.4.1. Soil hydraulic properties

Soil hydraulic properties were modeled using the van Genuchten–Mualem model as follows (van Genuchten, 1980).

$$\theta(h) = \theta_r + \frac{\theta_s - \theta_r}{[1 + (\alpha h)^n]^m} \qquad h < 0 \quad (8)$$

$$\theta(h) = \theta_s \qquad h \geq 0 \quad (9)$$

$$K(h) = K_s S_e^l \left[1 - (1 - S_e^{1/m})^m \right]^2 \quad (10)$$

where θ_s is saturated water content (L^3 L^{-3}), θ_r is residual water content (L^3 L^{-3}), m (-), n (-), and α (L^{-1}) are empirical parameters, K_s is saturated hydraulic conductivity (L T^{-1}), l is the pore connectivity parameter (-) taken as 0.5 (Mualem, 1976), and S_e is the effective saturation water content (-) as follows (van Genuchten, 1980).

$$S_e = \frac{\theta - \theta_r}{\theta_s - \theta_r}. \quad (11)$$

The soil hydraulic properties were estimated using Rosetta code implemented in HYDRUS using the measured data including bulk density, water content at field capacity, permanent wilting point and soil particle size distribution. Further, an inverse solution was performed to calculate the soil hydraulic properties using the measured water contents. The most sensitive parameters (K_s, θ_s and n) were found and the other parameters (θ_r and α) were considered equal to values obtained by the RETC program. The initial values of the soil hydraulic parameters were obtained in two ways; first, by fitting the observed retention data to the van Genuchten–Mualem model using RETC software, second by Rosetta. Since there was no significant difference between θ_r and α using RETC and Rosetta code' results, those parameters were considered fixed in the simulation process of soil moisture content. The initial values of θ_s, K_s, and n were considered based on the Rosetta code.

2.4.2. Flow domain and finite elements mesh

The transport domain simulated our lysimeter setup as 55 cm deep and 35 cm wide, with the dripper simulated at 20 cm below the soil surface. The dripper (located on the left vertical boundary of the transport domain (Fig. 1)) was represented as a half circle with a radius of 1 cm in all cases. For all simulations processes, we hypothesized that the soil was homogeneous so water flow was symmetrical in the horizontal direction and only one-half of the domain was simulated (Kandelous et al., 2012; Provenzano, 2007).

2.4.3. Initial and boundary condition

The initial soil water content, as an initial boundary condition, was considered fixed in the whole domain that corresponded to the measured soil water content before starting the first irrigation. The time variable flux boundary condition was considered using a half-circle at 20 cm depth, the dripper position. The dripper had constant flux for each irrigation. A zero water flux condition was assigned during the redistribution phase when water application was stopped, then an atmospheric boundary condition was assumed on the soil surface, a free drainage boundary condition was set for the probable drainage at the bottom of the soil, and a no-flow boundary condition was set along the right and left of the domain geometry. For solute transport, the third type Cauchy boundary condition was applied to the node's representing the dripper. For all treatments, the initial bacteria concentration in the soil was fixed to zero.

2.5. Statistical analysis

Modeling performance was evaluated for water flow and bacteria concentration using root mean square error (RMSE), regression coefficient (R^2), and mean absolute error (MAE) which were determined by:

$$RMSE = \sqrt{\frac{\sum_{i=1}^{n}(O_i - P_i)^2}{n}} \tag{12}$$

$$R^2 = 1 - \frac{\sum_{i=1}^{n}(P_i - O_i)^2}{\sum_{i=1}^{n}(O_i - \bar{O}_i)^2} \tag{13}$$

$$MAE = \frac{\sum_{i=1}^{n}|P_i - O_i|}{n \times O_i} \tag{14}$$

where O_i, P_i, and $\bar{O_i}$ respectively represent the observed, predicted, and the average of either water content or bacteria concentration, and n is the number of observations (Willmott, 1982).

3. Results and discussion

3.1. Biochar treated-soil properties

The soil texture was clay loam with a particle size distribution of 36.5% sand, 35.6% silt, and 27.9% clay. EC was 0.112 ± 0.008 dS m^{-1} for control soil, 0.43 ± 0.05 dS m^{-1} for biochar, 0.133 ± 0.027 dS m^{-1} for 0.5% biochar treated soil and 0.135 ± 0.01 dS m^{-1} for 1% biochar treated soil. Due to biochar particle density, bulk density decreased slightly from 1.31 ± 0.02 g cm^{-3} to 1.3 ± 0.009 g cm^{-3} and 1.29 ± 0.008 g cm^{-3} for the biochar treated soil at rates 0.5% and 1%, respectively. The specific surface area was 30.2 m^2 g^{-1} for the soil and 9.6 m^2 g^{-1} for the biochar. Biochar had a pH of 7.37 compared to the soil with a pH of 8.07, resulting in a slight decrease of pH to 7.6 ± 0.25 for 0.5% and 7.7 ± 0.12 for 1% biochar amended soil. A decrease of pH (11.7–3.7%) in an agricultural soil after addition of biochar-based fertilizer was also observed by Das and Ghosh (2021).

The value of θ_{fc} increased slightly after the addition of biochar, from 0.350 cm^3 cm^{-3} in the control to 0.358 and 0.365 cm^3 cm^{-3} for treatments mixed with 0.5 and 1% biochar, respectively. At the dry end of water retention, the θ_{pwp} value remained unchanged at about 0.17 cm^3 cm^{-3}. Biochar amendment of soil at a rate of 1% increased water retention slightly by 9% over the matric potentials range 0 to −700 cm. Simulations showed that soil hydraulic properties, including θ_s and θ_r, K_s, n, α, and l were not influenced by the addition of biochar (Table 1), as indicated in previous studies.

Major et al. (2012) reported that the addition of biochar produced from wood and applied at 20 t ha^{-1} to a clay soil had no significant effect on soil water retention and saturated hydraulic conductivity. Also, Jeffery et al. (2015) found that water retention and saturated hydraulic conductivity of a sandy soil did not significantly change after the addition of biochar produced from herbaceous feedstock at two temperatures (400 and 600 °C) and rates as high as 50 t ha^{-1}. Similarly, Hardie et al. (2014) found that incorporation of 47 t ha^{-1} biochar of acacia green waste into a sandy soil did not significantly alter soil hydraulic properties modeled using a bimodal van Genuchten–Mualemmodel. Rabbi et al. (2021) also found no distinct relation between type of biochar, its application rate and soil hydraulic properties.

However, in contrast with our results, Wu et al.'s (2019) study of a clay soil evaluated using the van Genuchten (1980) model showed that application of corn straw biochar at rates of 0, 25, 50, 75, and 100 t ha^{-1} could increase the values of θ_s and α, while, the values of n and θ_r parameters decreased with increasing biochar application. Also, in a pot experiment, Libutti et al. (2021) observed no change in tendency for the values of θ_r and α parameters of clay loam soil-biochar mixtures (0, 2, 4, 6, 8, and 10% w/w), but an increase for the θ_s and n parameters following the enhancement of biochar application rate. Lim et al. (2016) reported a decrease of the value of K_s for a clay loam soil after the addition of 1% and 2% (w/w) biochar produced from different feedstock materials (hardwood wood pellets, pine wood chips and hardwood chip), while addition of biochar at 5% had no effect. A similar finding was also reported by Kameyama et al. (2012); an increase of the θ_s values for an addition of 10% w/w biochar derived from sugarcane bagasse to a clay soil. Overall, studies demonstrate that the conflicting biochar results and impacts on soil properties and soil water retention are due to the

particle size and hydrophobicity, which depend on the type of biochar feedstocks (Herath et al., 2013; Edeh and Mašek, 2021).

An increase of saturated hydraulic conductivity in biochar amended soil has been attributed to increased tortuosity and macro-porosity due to greater soil aggregation (Lim et al., 2016; Major et al., 2012). Enhanced water retention could be due to intrapore (pores within the biochar structure) and interpore (formed between the biochar particles and the soil particles) (Libutti et al., 2021).

3.2. Model calibration using water flow

The agreement between the observed and simulated soil water content for model calibration was excellent; for *q*, RMSE (0.038 to 0.053), MAE (0.028–0.043) and R^2 (0.63–0.75), and for *Q*, RMSE (0.037 to 0.053), MAE (0.026–0.043) and R^2 (0.69–0.78). These results indicated that HYDRUS–2D can be successfully used to predict the variation of soil water content under subsurface drip irrigation in different conditions by applying a deterministic approach for simulating soil water movement based on the Richardson–Richards equation (Karandish and Simunek, 2016), agreeing with findings from other studies Arbat et al. (2020), and Kandelous and Šimůnek (2010b). The evaluation of wetting fronts for the control soils showed that the *q* rate had a larger lateral advancement compared to the *Q* rate, but there was not a significant difference between the *q* and *Q* rates for the vertical direction (see Supplementary data). However, the biochar-treated soils had smaller lateral and vertical wetting fronts if compared with unamended soil. Pu et al. (2019) also reported that the dimension of the wetting front decreased after the addition of 1, 2 and 4% biochar to soil. Skaggs et al. (2010) reported that diminishing the applied discharge rates for the subsurface drip irrigation leads to an increase of lateral spreading of the wetting front. This could impact soil water holding capacity and water distribution.

The mean values of the observed and simulated water content for the two layers of the lysimeters (0–20 and 20–55 cm) are illustrated in Fig. 2. The simulations both underestimated and overestimated water content for some points (*e.g.,* 0.242 vs. 0.234 cm^3 cm^{-3} in qM70B1: 0–20 cm or e.g., 0.246 vs. 0.272 cm^3 cm^{-3} in qM70B0.5: 20–55 cm). In most cases, particularly in the first and second irrigation events, the amount of simulated water content at 0–20 cm and 20–55 cm for the treatments was less than observations. This could be due to the drier water content simulated in the horizontal direction at 17 and 29 cm compared to the measured water content. Honari et al. (2017) and Grecco et al. (2019) found wetter simulated water contents at the points under the dripper compared to the other measured locations. Grecco et al. (2019) demonstrated that HYDRUS–2D simulated wetter water contents of the first layer of soil (0–25 cm) before and at the time of irrigations (0 to 110 days) compared to the observed data, but after this period the model underestimated water contents before irrigations. The differences in the coordinate of the TDR probes and the observation nodes in the model were considered as the reason for these results. In comparison, they noted that the water contents of the second layer (25–50 cm) was simulated better. Another study by Xi et al. (2016) found large differences between the observed soil water contents and the simulated ones using HYDRUS–2D under a subsurface drip irrigation of a silt soil at depth of 0–20 cm. In our study, the difference between measured and simulated water content in soil treated with biochar after stoppage of irrigation was less than for unamended soil. This may be associated with uncertainties in optimization, because of an increase in water retention of the amended soils than the unamended ones, however, further research would be needed to find the main reason.

3.3. Modeling bacteria scenarios

Four scenarios were considered to determine the most possible mechanism(s) for transport and retention of bacteria through the studied soils: (i) in the first scenario, we estimated attachment, straining, and physical detachment coefficient (*i.e.,* only for the first site) coefficients; (ii) then in the second scenario, bacteria inactivation was estimated for the solid and aqueous phases with regards to the inversed attachment, detachment and straining in the first scenario considered fixed; (iii) afterward, bacteria inactivation process in the solid and liquid phases was assessed without considering the retention and transport mechanisms; and (iv) finally in the fourth scenario, the coefficients of attachment, straining, and physical detachment, as well as the inactivation coefficient were simultaneously estimated (see Tables 2–5).

The results from the first scenario showed that the k_{str} was at least 10^3 times and at most 10^6 times higher than the k_{att} values. The k_{det} coefficient (i.e., for the first site) was smaller than k_{str} indicating that straining was the dominant mechanism for transport and retention of bacteria in all treatments. The highest and lowest values of k_{str} were for qM70B1 and qM30B0.5, respectively. The physicochemical detachment coefficient (*i.e.,* for the second site) was not considered due to the very small values of the k_{att} simulated. The range of R^2 was 0.86 to 0.98, RMSE was 0.017 to 0.057, and MAE was 0.01 to 0.027.

From the second scenario, bacteria growth and die-off was affected by the 30 days irrigation duration of each treatment in the experiment. The results indicated that the inactivation rate in the solid phase was higher than in the liquid phase, which corresponded with the first scenario, where straining was found as the main retention mechanism. The range of R^2 was 0.81 to 0.98, RMSE was 0.017 to 0.057 and MAE was 0.009 to 0.026.

However, in the third scenario, the values of the inversed inactivation coefficient in the liquid phase were much higher than in the solid phase, and not within the ranges of previous reports (e.g. Schijven and Šimůnek, 2002). Amin et al. (2014) found this value could be changed between 0.1 to 0.12 day^{-1} for *E. coli* in a sandy loam and a sandy clay loam. Morales

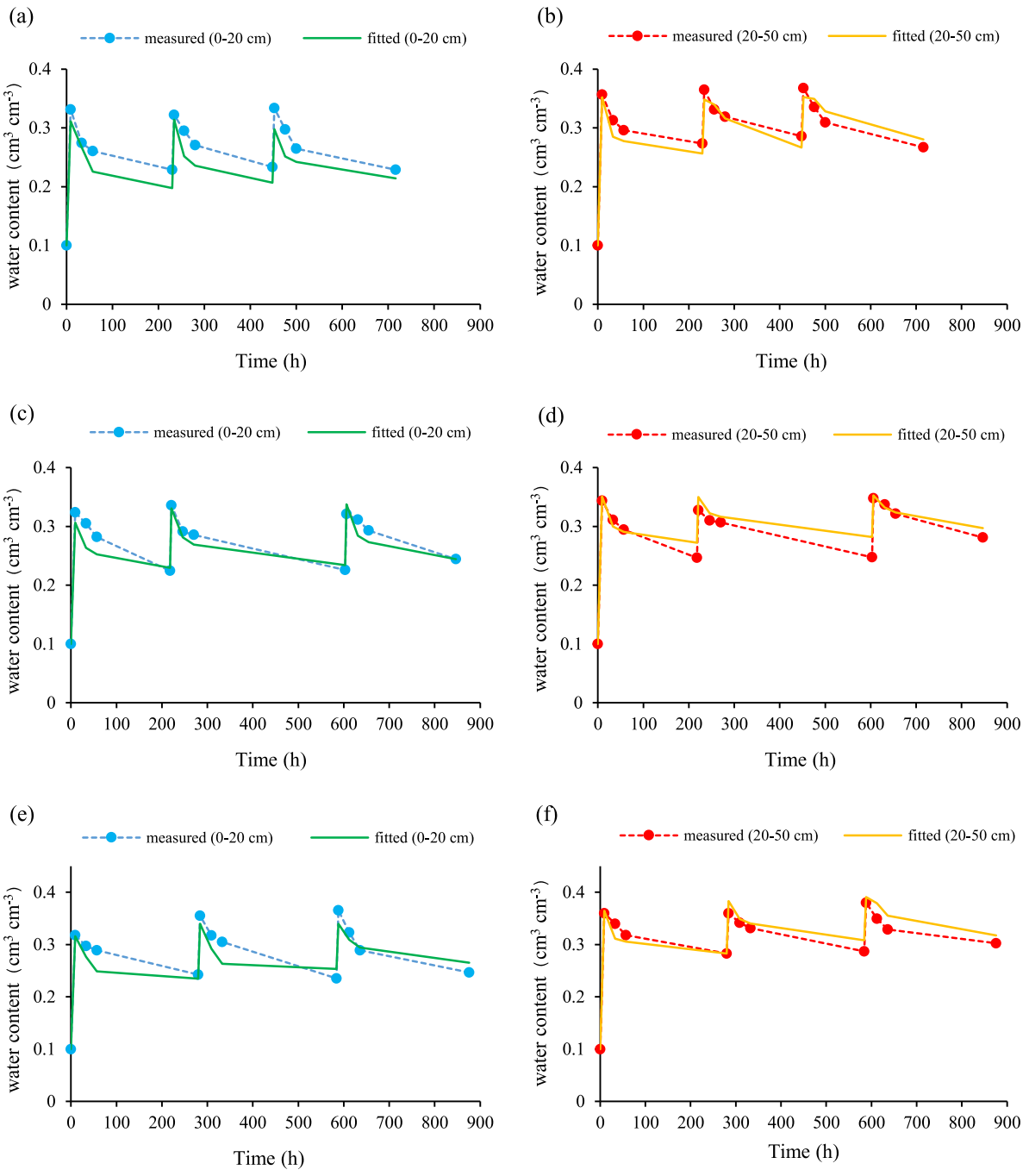

Fig. 2. Observed and fitted soil water content during experiment: (a) and (b) qM70B0; (c) and (d) qM70B0.5; (e) and (f) qM70B1. *q* indicates discharge rate 0.003 cm h^{-1}; M70 is MAD 70%; B0, 0.5, and 1 are biochar application rates 0, 0.5 and 1%, respectively.

et al. (2014) reported an *E. coli* die-off rate in the aqueous phase of about 0.0824 h^{-1} across a range of soil textures. The data for the bacteriophages showed that values of the inactivation coefficient in the liquid phase could range from 0.03 to 0.12 day^{-1} depending on bacteriophage in dune recharge, or 0.039 day^{-1} for removal of bacteriophage in deep well injection (Schijven and Šimůnek, 2002). Furthermore, Hassanizadeh and Schijven (2000) found that the inactivation coefficient varied from 0.03 to 0.06 day^{-1} for bacteriophage.

Estimation and optimization of many parameters are not recommended due to the uniqueness of problems using HYDRUS, but our results for the first and second scenarios were also confirmed in the last scenario. The results demonstrated the predominance of straining as the main mechanism in the retention of bacteria, regardless of the various

Table 2
First modeling scenario; transport and retention parameters (attachment coefficient k_{att}, straining coefficient k_{str}, and physical release k_{det}) for the studied soils.

Treatments	k_{att} (h^{-1})	k_{str} (h^{-1})	k_{det} (h^{-1})	R^2	RMSE	MAE
qM30B0	6.33×10^{-6}	2.236	0.608	0.97	0.023	0.012
qM30B0.5	1.58×10^{-5}	1.133	0.275	0.95	0.031	0.015
qM30B1	3.13×10^{-6}	2.000	0.504	0.92	0.037	0.018
qM50B0	5.40×10^{-6}	2.340	0.633	0.96	0.025	0.013
qM50B0.5	1.70×10^{-4}	2.756	0.706	0.97	0.023	0.012
qM50B1	2.99×10^{-3}	1.355	0.356	0.98	0.020	0.011
qM70B0	3.26×10^{-6}	2.190	0.556	0.97	0.057	0.025
qM70B0.5	1.00×10^{-3}	4.622	1.189	0.96	0.030	0.015
qM70B1	3.10×10^{-6}	5.828	1.524	0.97	0.025	0.012
QM30B0	8.30×10^{-6}	2.214	0.605	0.95	0.033	0.019
QM30B0.5	4.06×10^{-5}	1.619	0.417	0.86	0.057	0.027
QM30B1	1.73×10^{-5}	2.507	0.639	0.92	0.035	0.018
QM50B0	1.15×10^{-6}	1.211	0.321	0.95	0.040	0.025
QM50B0.5	3.13×10^{-6}	3.376	0.939	0.96	0.025	0.012
QM50B1	3.19×10^{-3}	2.243	0.576	0.98	0.048	0.019
QM70B0	1.49×10^{-3}	1.543	0.433	0.97	0.024	0.014
QM70B0.5	8.73×10^{-4}	1.972	0.542	0.98	0.017	0.010
QM70B1	4.73×10^{-6}	1.740	0.485	0.98	0.032	0.021

q and *Q* indicate discharge rates 0.003 and 0.0064 cm h^{-1}; M30, 50, and 70 are MAD30, 50 and 70%; B0, 0.5, and 1 are biochar application rates 0, 0.5, and 1 %, respectively.

Table 3
Second modeling scenario; inactivation coefficients for the liquid (μ_l) and solid (μ_s) phases with regards to the fixed attachment coefficient (k_{att}), straining coefficient (k_{str}), and physical release (k_{det}) yielded from the first scenario.

Treatments	k_{att} (h^{-1})	k_{str} (h^{-1})	k_{det} (h^{-1})	μ_l (h^{-1})	μ_s (h^{-1})	R^2	RMSE	MAE
qM30B0	6.33×10^{-6}	2.236	0.608	2.45×10^{-6}	2.89×10^{-6}	0.97	0.030	0.016
qM30B0.5	1.58×10^{-5}	1.133	0.275	1.28×10^{-6}	9.6×10^{-5}	0.94	0.031	0.016
qM30B1	3.13×10^{-6}	2.00	0.504	1.18×10^{-5}	3.46×10^{-6}	0.92	0.037	0.018
qM50B0	5.40×10^{-6}	2.34	0.633	1.35×10^{-7}	7.81×10^{-7}	0.97	0.050	0.022
qM50B0.5	1.70×10^{-4}	2.756	0.706	4.12×10^{-5}	1.31×10^{-6}	0.97	0.023	0.012
qM50B1	2.99×10^{-3}	1.355	0.355	4.18×10^{-6}	3.13×10^{-6}	0.98	0.020	0.011
qM70B0	3.26×10^{-6}	2.190	0.556	4.88×10^{-7}	4.56×10^{-6}	0.97	0.057	0.026
qM70B0.5	1.00×10^{-3}	4.622	1.189	4.12×10^{-5}	4.22×10^{-6}	0.96	0.025	0.012
qM70B1	3.10×10^{-6}	5.828	1.524	1.87×10^{-6}	7.96×10^{-6}	0.97	0.025	0.012
QM30B0	8.30×10^{-6}	2.214	0.605	8.50×10^{-7}	9.80×10^{-5}	0.96	0.047	0.024
QM30B0.5	4.06×10^{-5}	1.619	0.417	5.54×10^{-6}	3.14×10^{-6}	0.81	0.056	0.026
QM30B1	1.73×10^{-5}	2.507	0.639	4.88×10^{-6}	3.20×10^{-6}	0.92	0.035	0.018
QM50B0	1.15×10^{-6}	1.211	0.321	4.30×10^{-7}	4.96×10^{-8}	0.95	0.040	0.025
QM50B0.5	3.13×10^{-6}	3.376	0.939	6.47×10^{-8}	3.14×10^{-6}	0.96	0.025	0.013
QM50B1	3.19×10^{-3}	2.243	0.576	1.28×10^{-4}	9.36×10^{-5}	0.98	0.017	0.009
QM70B0	1.49×10^{-3}	1.543	0.433	2.72×10^{-5}	2.78×10^{-6}	0.96	0.024	0.014
QM70B0.5	8.73×10^{-4}	1.972	0.542	2.07×10^{-6}	3.91×10^{-6}	0.98	0.017	0.010
QM70B1	2.70×10^{-6}	1.626	0.435	1.18×10^{-5}	9.26×10^{-5}	0.97	0.022	0.012

q and *Q* indicate discharge rates 0.003 and 0.0064 cm h^{-1}; M30, 50, and 70 are MAD30, 50 and 70%; B0, 0.5, and 1 are biochar application rates 0, 0.5, and 1 %, respectively.

treatments applied (Table 5). Modeling showed that bio-colloids can be removed from the solid phase by first-order entrainment and inactivation, and by attachment to the solid phase from the liquid phase. Furthermore, the data illustrated the greater values of the inactivation coefficient in the solid phase than in the aqueous phase. Morales et al. (2014) also reported a similar result; a higher bacteria die-off rate in the solid phase than the liquid phase of a clay loam soil.

The values of the k_{str} were several times higher than the k_{att} for our biochar amendment treatments, and the straining coefficients were higher than the physical detachments coefficients. This demonstrates that, under our experiments conditions (*i.e.,* time, biochar, flow interruption, and discharge rate), straining was the main mechanism in the removal of bacteria from the irrigation water. Even larger values of k_{str} compared to k_{att} for *E. coli (ATCC 25255)* and *Klebsiella oxytoca* were obtained using HYDRUS–1D in a study by Bai et al. (2016) through fine sandy and coarse sandy column. In addition, studies have shown that straining can be an effective mechanism for inhibiting extracellular antibiotic resistance genes (eARGs) mobility in quartz sandy columns amended with biochar (700 °C) (e.g., Fang et al., 2022). The R^2 varied between

Table 4
Third modeling scenario; inactivation rates for the liquid (μ_l) and solid (μ_s) phases without attachment coefficient (k_{att}), straining coefficient (k_{str}), and physical release (k_{det}).

Treatments	k_{att} (h^{-1})	k_{str} (h^{-1})	k_{det} (h^{-1})	μ_l (h^{-1})	μ_s (h^{-1})	R^2	RMSE	MAE
qM30B0	–	–	–	1.34×10^{2}	1.00×10^{-3}	0.29	0.177	0.104
qM30B0.5	–	–	–	1.05×10^{2}	2.00×10^{-4}	0.26	0.169	0.099
qM30B1	–	–	–	1.00	4.00×10^{-3}	0.32	0.18	0.102
qM50B0	–	–	–	1.34×10^{2}	1.00×10^{-1}	0.03	0.59	0.23
qM50B0.5	–	–	–	1.00	2.00×10^{-3}	0.34	0.097	0.177
qM50B1	–	–	–	1.00×10^{2}	1.00×10^{-1}	0.15	0.16	0.092
qM70B0	–	–	–	7.95×10^{1}	1.00×10^{-2}	0.002	0.58	0.23
qM70B0.5	–	–	–	1.06×10^{2}	1.00×10^{-3}	0.29	0.157	0.088
qM70B1	–	–	–	1.62	1.00×10^{-3}	0.41	0.181	0.098
QM30B0	–	–	–	1.64×10^{1}	1.00×10^{-3}	0.20	0.212	0.138
QM30B0.5	–	–	–	1.69×10^{1}	1.00×10^{-4}	0.07	0.16	0.092
QM30B1	–	–	–	1.18	1.00×10^{-3}	0.20	0.161	0.094
QM50B0	–	–	–	1.69×10^{1}	1.00×10^{-3}	0.46	0.342	0.172
QM50B0.5	–	–	–	1.99×10^{1}	2.89×10^{-4}	0.26	0.16	0.092
QM50B1	–	–	–	1.94×10^{2}	1.00×10^{-3}	0.136	0.161	0.094
QM70B0	–	–	–	5.34×10^{1}	1.00	0.09	0.168	0.097
QM70B0.5	–	–	–	1.66×10^{1}	1.00×10^{-3}	0.116	0.159	0.091
QM70B1	–	–	–	1.93×10^{2}	1.00×10^{-4}	0.188	0.161	0.094

q and Q indicate discharge rates 0.003 and 0.0064 cm h^{-1}; M30, 50, and 70 are MAD 30, 50 and 70%; B0, 0.5, and 1 are biochar application rates 0, 0.5, and 1 %, respectively.

Table 5
Fourth modeling scenario; transport and retention parameters including attachment coefficient (k_{att}), straining coefficient (k_{str}), physical release (k_{det}) and inactivation coefficients for the liquid (μ_l) and solid (μ_s) phases of the studied soils.

Treatments	k_{att} (h^{-1})	k_{str} (h^{-1})	k_{det} (h^{-1})	μ_l (h^{-1})	μ_s (h^{-1})	R^2	RMSE	MAE
qM30B0	1.85×10^{-3}	0.917	0.207	3.96×10^{-6}	1.27×10^{-3}	0.95	0.039	0.016
qM30B0.5	4.11×10^{-6}	0.743	0.150	3.00×10^{-6}	2.18×10^{-3}	0.90	0.042	0.021
qM30B1	2.85×10^{-4}	0.934	0.197	1.37×10^{-5}	1.78×10^{-3}	0.88	0.043	0.021
qM50B0	7.56×10^{-5}	1.016	0.241	6.50×10^{-6}	1.63×10^{-3}	0.94	0.040	0.020
qM50B0.5	1.69×10^{-4}	1.042	0.231	5.20×10^{-5}	1.23×10^{-3}	0.95	0.028	0.014
qM50B1	1.13×10^{-3}	1.357	0.353	1.69×10^{-5}	6.42×10^{-4}	0.98	0.02	0.011
qM70B0	3.34×10^{-5}	1.701	0.414	2.21×10^{-5}	1.45×10^{-3}	0.95	0.027	0.014
qM70B0.5	1.77×10^{-5}	1.909	0.455	2.85×10^{-3}	3.20×10^{-4}	0.95	0.032	0.018
qM70B1	2.95×10^{-5}	1.229	0.287	1.67×10^{-6}	1.73×10^{-4}	0.94	0.033	0.017
QM30B0	3.41×10^{-6}	1.246	0.281	1.51×10^{-6}	2.58×10^{-3}	0.94	0.050	0.028
QM30B0.5	2.53×10^{-5}	1.309	0.311	8.32×10^{-4}	8.95×10^{-4}	0.81	0.057	0.026
QM30B1	8.17×10^{-6}	1.357	0.334	7.50×10^{-6}	3.61×10^{-5}	0.93	0.058	0.026
QM50B0	2.84×10^{-4}	1.356	0.361	3.57×10^{-5}	1.81×10^{-3}	0.92	0.050	0.029
QM50B0.5	3.12×10^{-6}	2.298	0.621	4.58×10^{-5}	2.37×10^{-4}	0.96	0.026	0.014
QM50B1	1.27×10^{-4}	1.967	0.501	6.84×10^{-5}	8.50×10^{-4}	0.98	0.017	0.009
QM70B0	6.18×10^{-7}	1.527	0.427	5.98×10^{-4}	2.61×10^{-4}	0.97	0.024	0.014
QM70B0.5	3.13×10^{-6}	1.937	0.531	1.18×10^{-4}	2.18×10^{-4}	0.98	0.017	0.01
QM70B1	8.31×10^{-6}	1.709	0.468	1.25×10^{-7}	1.76×10^{-5}	0.97	0.021	0.012

q and Q indicate discharge rates 0.003 and 0.0064 cm h^{-1}; M30, 50, and 70 are MAD 30, 50 and 70%; B0, 0.5, and 1 are biochar application rates 0, 0.5 and 1 %, respectively.

0.81 and 0.98 and the values of RMSE and MAE ranged from 0.017 to 0.058 and 0.0095 to 0.029, respectively. With this illustration, the differences between the various treatments are discussed in detail in the following based on scenario iv.

3.4. Bacteria straining and die-off

Our scenario iv (estimation of attachment, straining, and physical detachment coefficients, as well as the inactivation coefficient) showed that straining and die-off controlled bacteria retention through the biochar-treated soils and the control soils. The bacteria mortality for the applied biochar at rates of 0, 0.5 and 1% were 7.99×10^{-4}, 7.25×10^{-4}, and 3.01×10^{-4} h^{-1}, respectively, demonstrating that biochar can retain and protect bacteria in soil (Pang et al., 2008). Bacteria straining was higher for the Q compared with q, indicating that the higher flow rate forced bacteria into the biochar pore spaces, and resulted in a decrease of bacteria die-off. On the other hand, for the q, the effect of clay content for the various treatments was higher, because the q resulted in a longer contact time and therefore a higher bacteria attachment and most probably bacteria collision on particle surfaces.

The k_{att} for the q and Q treatments varied between 4.11×10^{-6} to 1.85×10^{-3} h^{-1} and 3.13×10^{-6} to 5.55×10^{-4} h^{-1}, respectively. The smallest and the largest values of this coefficient under the q were related to the M30B0.5 and M30B0, respectively. This not only shows the negligible effect of biochar on bacteria attachment, but also illustrates clear evidence of bacteria retention as the result of straining (*i.e.,* bacteria trapping in biochar pores, but not on its surfaces). However, the simultaneous effects of clay content and low water flow led to various k_{att} values for the treatments for MADs so that we could not thus find an obvious link between the attachment coefficients for the applied biochar rates. For the Q treated ones, the differences of k_{att} decreased between the treatments indicating an obvious effect of water flow on bacteria retention. Furthermore, for this flow discharge rate, the k_{att} values increased as the soil dried in term of the MADs (*e.g.,* MAD70%). Overall, the highest values of k_{att} and k_{str} were related to the q and the Q, respectively, furthermore, the flow rate and biochar had higher effects on bacteria retention and inactivation than the MADs. The smallest values of k_{str} were observed for the irrigation with short frequency (*i.e.,* MAD 30%) in both of q and Q treatments. Madumathi et al. (2017) reported that an increase of flow velocity in sand and soil columns from 0.0535 to 0.214 (cm h^{-1}), decreased the attachment coefficient for 4.4% and 1.1%, respectively. Some studies indicated that for soils with smaller pore size, high clay, and organic matter contents, straining can be the main mechanism for colloid retention (Bradford et al., 2013; Pang et al., 2008). In other studies the interaction between clay particles and pore structure (Abit et al., 2014) or soil aggregate formation and system hydrodynamics (Gargiulo et al., 2007) have been shown to increase bacterial straining. Our study with biochar shows that its interaction with soil pore structure and surface area also affects bacteria straining.

The detachment data illustrated that the treatments under Q had the higher values of the k_{det} than the q counterparts, so that the largest and the smallest values of physical detachment related to QM50B0.5 and qM30B0.5, respectively. The larger values of the k_{det} and the increase of soil water holding capacity in biochar-amended soils (*i.e.,* 1% biochar application rate) indicated the occurrence of physical release in the biochar pores. As discussed earlier (see Section 3.2.), addition of biochar enhanced soil mesopores and macropores, therefore, flowing water through soil macropores could trap bacteria in those pores due to the larger size. But, the higher values of the k_{det} for the Q than the q might be due the higher hydrodynamic shear force that might alter water flow behavior at the pore scale so that trapped bacteria in the pores are remobilized (Engström et al., 2015).

3.5. Bacteria retention modes

The observed and simulated retention data are given in Figs. 3–5. The highest concentrations of bacteria at depths 15 and 25 cm were predicted very well by the model ($R^2 = 0.83$ to 0.97), but the model failed to simulate bacteria concentration at a depth of 50 cm (i.e., the bottom of the lysimeters) for all treatments. At this depth, the smallest bacteria concentration was observed at the beginning of irrigation but the greatest one at the end of experiments. This might indicate that further retention mechanism (e.g., ripening) could affect bacteria retention deeper in the soil (Zhong et al., 2017). However, our observations and simulations provided sufficient evidence that straining was the most important mechanism for bacteria retention across our treatments.

Bacteria retention profiles are shown in Fig. 6a–c. The retention profiles of all treatments exhibited a similar shape (i.e., bell shape), and the simulations correctly captured the four studied depths (0–5, 15, 25 and 50 cm) (Fig. 6a–c). However, the predicted amounts of bacteria particularly at depths 15, 25 and 50 cm were over-predicted compared to our observations that clearly showed the amounts of bacteria gradually decreasing after 12 days from the stoppage of the third irrigation (Figs. 3–5). The overestimations were higher for the treatments at 1% biochar compared to the other rates, possibly due to the smaller predicted inactivation coefficients. Uncertainties in survival rates of bacteria and preferential flow in different parts of soil can result in underestimation by HYDRUS–2D that fails to capture the experimental data (Amin et al., 2014).

4. Conclusion

Biochar was found to positively control bacteria transport from subsurface drip irrigation in soil over our 30 day controlled lysimeter study. The novel data generated allowed testing of HYDRUS–2D, with the combined experimental and modeling results indicating at 1% (w/w) biochar amendment, smaller MAD (e.g. 30%) and slower flow rates, bacteria retention was greatest and dominated by physical straining of the bacteria. Biochar likely had direct impacts by providing new macropore structure that strained bacteria, but the water retention data suggests that biochar also affected soil macropores through aggregation. A significant advancement for this study was confirmation that HYDRUS–2D effectively modeled bacteria transport, providing scope to upscale to field conditions and test a range of different scenarios.

Our research explored one soil and one type of biochar mixed at two concentrations. Clearly there are positive impacts of biochar on bacteria retention, especially at 1% (w/w) application levels, but testing could be expanded to explore whether pyrolysis temperature, and feedstock type of biochar could be optimized for even greater bacteria retention. With the growing use of treated wastewater for drip irrigation, technologies like biochar to mitigate bacteria transport are promising. With knowledge from more soils, HYDRUS–2D could be applied to predict impacts and therefore increase confidence in management decisions.

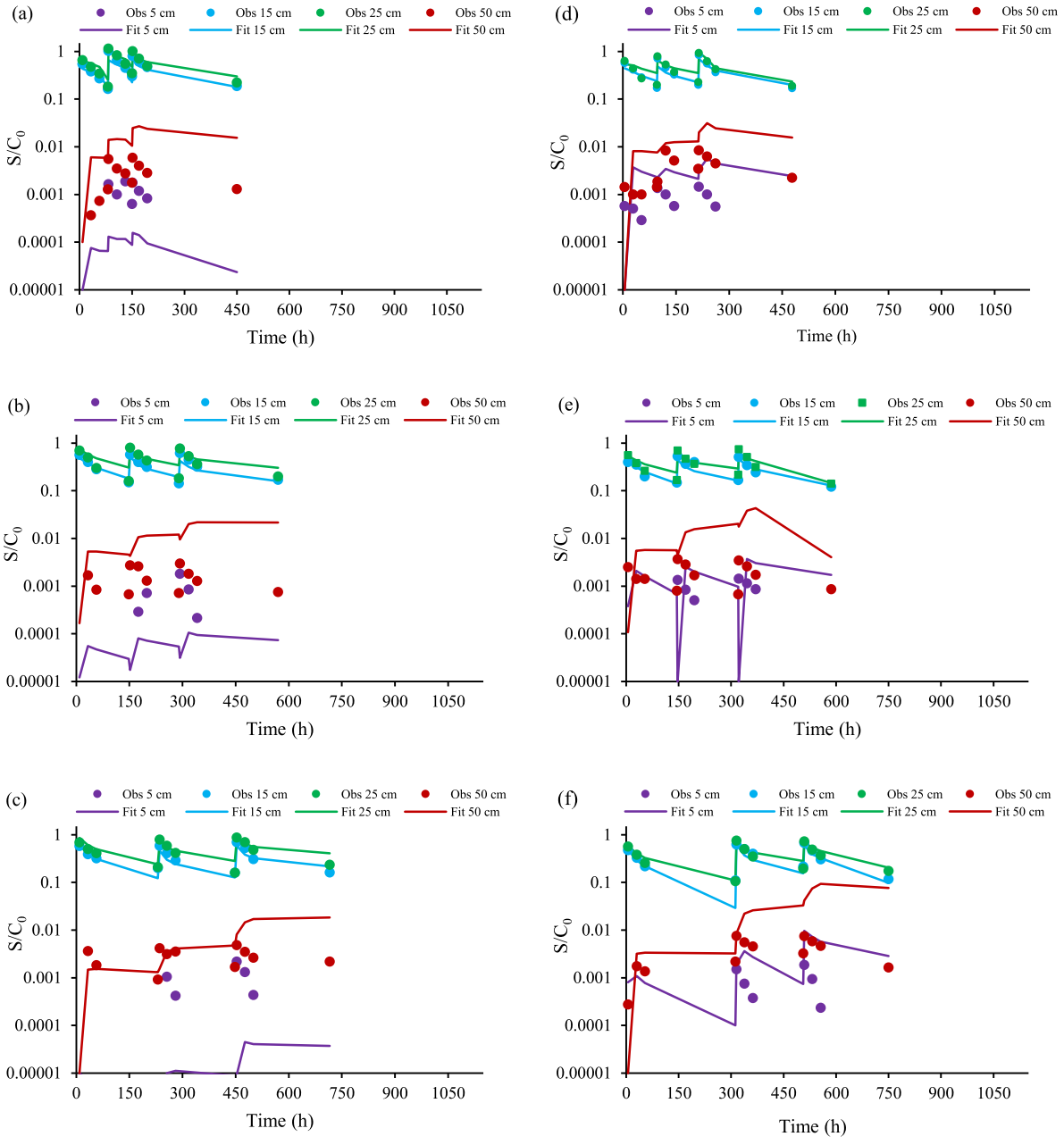

Fig. 3. Temporal–spatial distribution of bacteria under q and Q treatments: (a) qM30B0, (b) qM50B0, (c) qM70B0, (d) QM30B0, (e) QM50B0, (f) QM70B0. q and Q indicate discharge rates 0.003 and 0.0064 cm h^{-1}; M30, M50, and M70 are MAD 30, 50, and 70%, respectively; B0 is biochar application rate 0%.

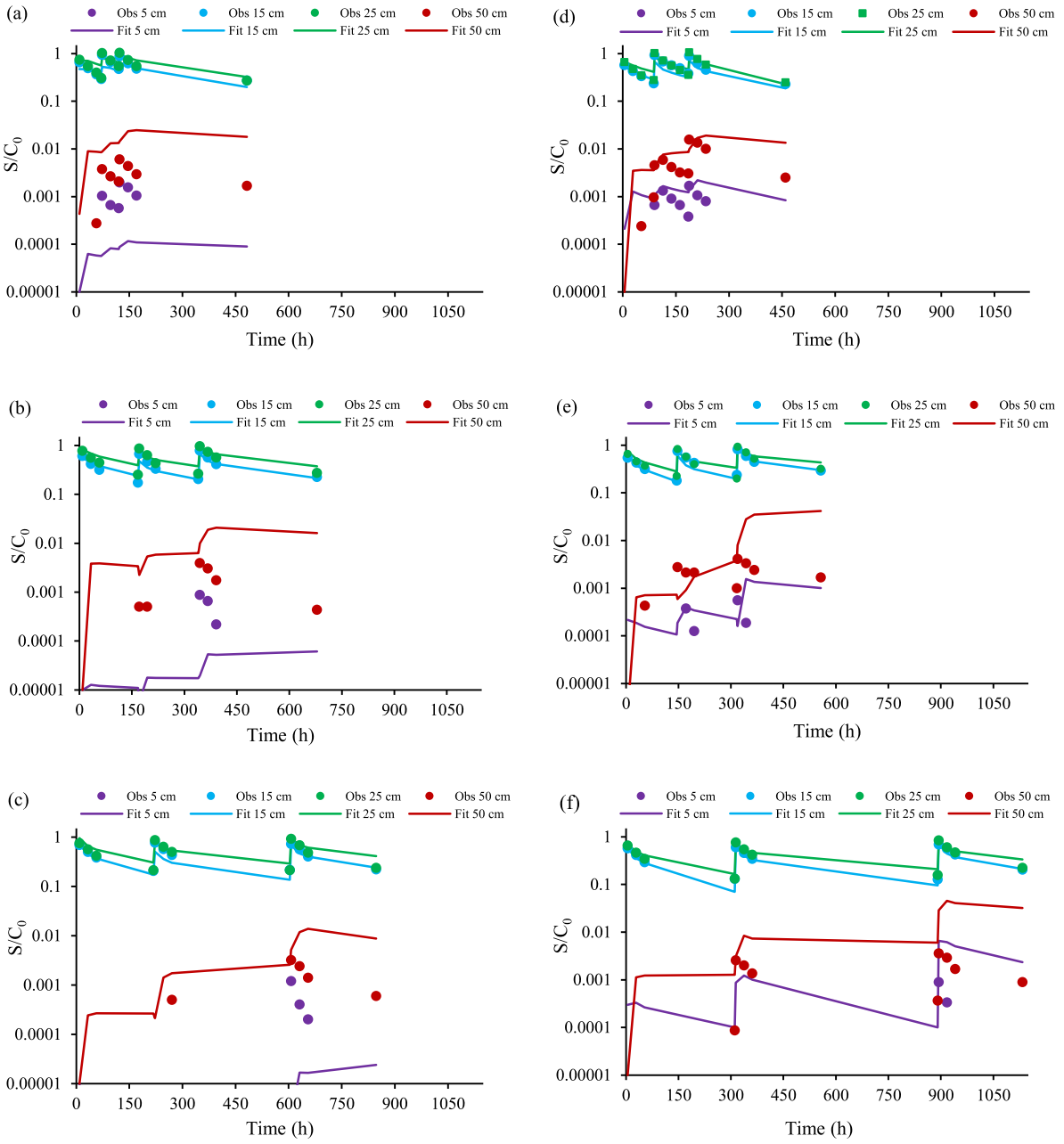

Fig. 4. Temporal–spatial distribution of bacteria under q and Q treatments: (a) qM30B0.5, (b) qM50B0.5, (c) qM70B0.5, (d) QM30B0.5, (e) QM50B0.5, (f) QM70B0.5. q and Q indicate discharge rates 0.003 and 0.0064 cm h^{-1}; M30, M50, and M70 are MAD 30, 50 and 70%, respectively; B0.5 is biochar application rate 0.5%.

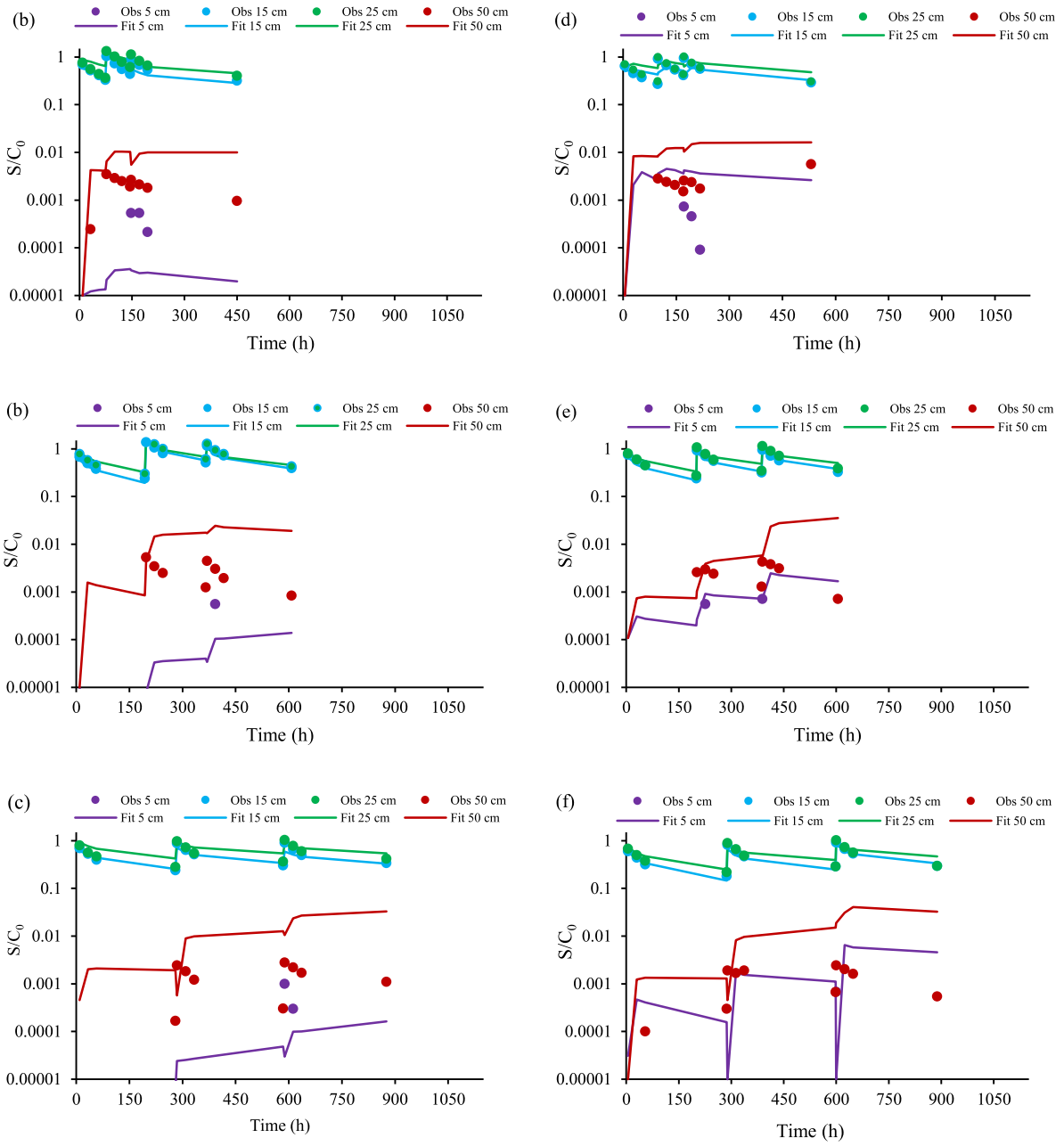

Fig. 5. Temporal–spatial distribution of bacteria under q and Q treatments: (a) qM30B1, (b) qM50B1, (c) qM70B1, (d) QM30B1, (e) QM50B1, (f) QM70B1. q and Q indicate discharge rates 0.003 and 0.0064 cm h^{-1}; M30, M50 and M70 are MAD 30, 50 and 70%, respectively; B1 is biochar application rate 1%.

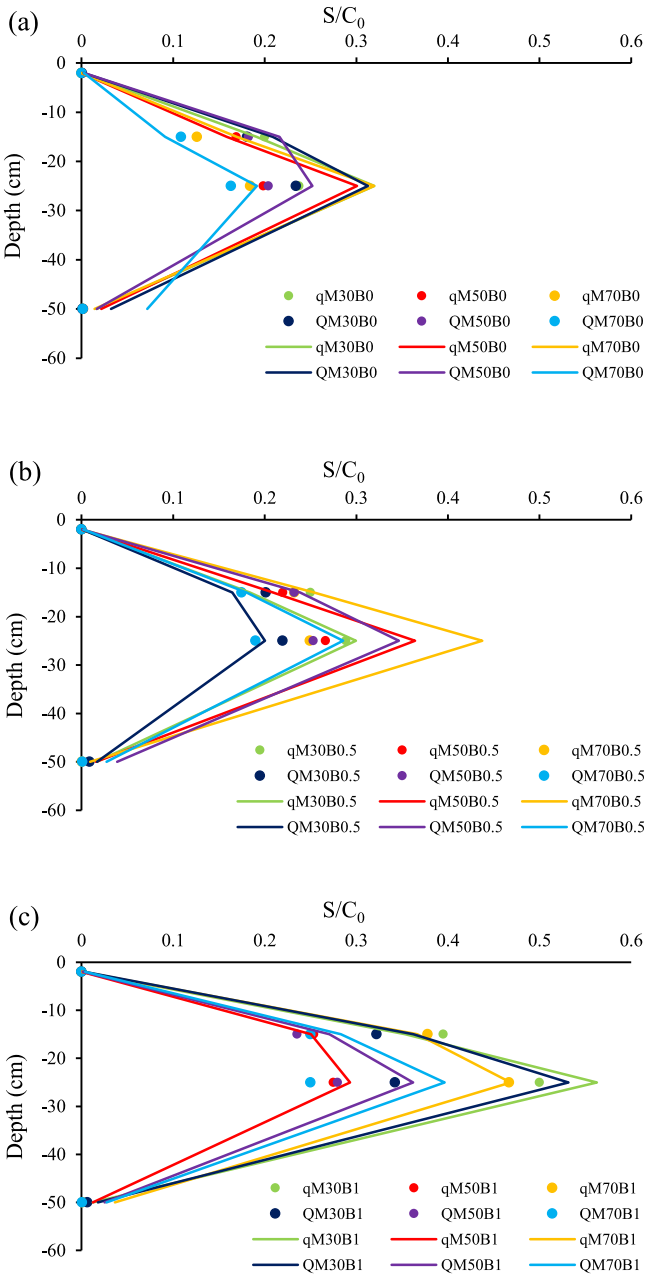

Fig. 6. Retention of fecal coliform at different soil depths for flow rates of q and Q cm h^{-1}; (a) control soil, (b) soil treated biochar (0.5%), and (c) soil treated biochar (1%). (Symbols and lines are observed and fitted data, respectively.) q and Q indicate discharge rate 0.003 and 0.0064 cm h^{-1}; M30, M50 and M70 are MAD 30, 50 and 70%; B0, 0.5, and 1 are biochar application rates 0, 0.5 and 1%, respectively.

CRediT authorship contribution statement

Forough Abbasi Teshnizi: Sampling, Preparation, Investigation, Data acquisition, Conceptualization, Methodology, Development of the original idea, Formal analysis, Writing – original draft, Writing – review & editing. **Mahdi Ghobadinia:** Conceptualization, Development of the original idea. **Fariborz Abbasi:** Conceptualication. **Paul D. Hallett:** Conceptualization, Development of the original idea, Data validation, Writing – review & editing. **Nasrollah Sepehrnia:** Conceptualization, Development of the original idea, Data validation, Writing – review & editing.

Declaration of competing interest

The authors declare that they have no known competing financial interests or personal relationships that could have appeared to influence the work reported in this paper.

Data availability

Data will be made available on request.

Acknowledgments

This work was supported by Shahrekord University, Iran. N. Sepehrnia is funded by a Marie Skłodowska-Curie Individual Fellowship, United Kingdom under the grant agreement No. 101026287. We acknowledge University of Aberdeen, UK for supporting this project.

Appendix A. Supplementary data

Supplementary material related to this article can be found online at https://doi.org/10.1016/j.eti.2023.103229.

References

Abel, S., Peters, A., Trinks, S., Schonsky, H., Facklam, M., Wessolek, G., 2013. Impact of biochar and hydrochar addition on water retention and water repellency of sandy soil. Geoderma 202–203, 183–191. http://dx.doi.org/10.1016/j.geoderma.2013.03.003.

Abit, S.M., Bolster, C.H., Cantrell, K.B., Flores, J.Q., Walker, S.L., 2014. Transport of Escherichia coli, Salmonella typhimurium, and Microspheres in biochar-amended soils with different textures. J. Environ. Qual. 43, 371–388. http://dx.doi.org/10.2134/jeq2013.06.0236.

Akhavan, S., Ebrahimi, S., Navabian, M., Shabanpour, M., Mojtahedi, A., Movahedi Naeini, A., 2018. Significance of physicochemical factors in the transmission of Escherichia coli and chloride. Environ. Heal. Eng. Manag. J 5, 115–122.

Aller, M.F., 2016. Biochar properties: transport, fate, and impact. Crit. Rev. Environ. Sci. Technol. 46, 1183–1296.

Amin, M.G.M., Šimůnek, J., Lægdsmand, M., 2014. Simulation of the redistribution and fate of contaminants from soil-injected animal slurry. Agric. Water Manag. 131, 17–29. http://dx.doi.org/10.1016/j.agwat.2013.09.002.

Arbat, G., Sílvia Cufí, M.D.-R., Pinsach, J., Puig-Bargués, J., De, C. co R., 2020. Modeling approaches for determining dripline depth and irrigation frequency of subsurface drip irrigated Rice on different soil textures. Water 12 (1724), http://dx.doi.org/10.3390/w12061724.

Arief Ismail, S., Prasher, S., Chénier, M., Patel, R., 2016. Evaluation of biochar soil amendments in reducing soil and water pollution from total and fecal coliforms in poultry manure. Can. Biosyst. Eng. 58, 1.21–1.31. http://dx.doi.org/10.7451/cbe.2016.58.1.21.

Bai, H., Cochet, N., Pauss, A., Lamy, E., 2016. Bacteria cell properties and grain size impact on bacteria transport and deposition in porous media. Colloids Surfaces B 139, 148–155.

Bolster, C.H., Abit, S.M., 2012. Biochar pyrolyzed at two temperatures affects Escherichia coli transport through a sandy soil. J. Environ. Qual. 41, 124–133.

Bradford, S.A., Morales, V.L., Zhang, W., Harvey, R.W., Packman, A.I., Mohanram, A., Welty, C., 2013. Transport and fate of microbial pathogens in agricultural settings. Crit. Rev. Environ. Sci. Technol. http://dx.doi.org/10.1080/10643389.2012.710449.

Bradford, S.A., Simunek, J., Bettahar, M., Van Genuchten, M.T., Yates, S.R., 2003. Modeling colloid attachment, straining, and exclusion in saturated porous media. Environ. Sci. Technol. 37, 2242–2250.

Brunauer, S., Emmett, P.H., Teller, E., 1938. Adsorption of gases in multimolecular layers. J. Am. Chem. Soc. 60, 309–319.

Cui, E., Fan, X., Li, Z., Liu, Y., Neal, A.L., Hu, C., Gao, F., 2019. Variations in soil and plant-microbiome composition with different quality irrigation waters and biochar supplementation. Appl. Soil Ecol. 142, 99–109.

Das, S.K., Ghosh, G.K., 2021. Developing biochar-based slow-release NPK fertilizer for controlled nutrient release and its impact on soil health and yield. Biomass Convers. Biorefinery 1–13.

Das, S.K., Ghosh, G.K., 2022. Conversion of biomass into low-cost biochar along with organic manure improved soil hydro-physical environment through technological intervention for sandy soil restoration. Biomass Convers. Biorefinery 1–13. http://dx.doi.org/10.1007/s13399-022-02724-6.

Edeh, I.G., Mašek, O., 2021. The role of biochar particle size and hydrophobicity in improving soil hydraulic properties. Eur. J. Soil Sci. 1–14.

Elasbah, R., Selim, T., Mirdan, A., Berndtsson, R., 2019. Modeling of fertilizer transport for various fertigation scenarios under drip irrigation. Water 11 (893).

Engström, E., Thunvik, R., Kulabako, R., Balfors, B., 2015. Water transport, retention, and survival of Escherichia coli in unsaturated porous media: A comprehensive review of processes, models, and factors. Environ. Sci. Technol. 45, 1–100. http://dx.doi.org/10.1080/10643389.2013.828363.

Fang, J., Li, W., Tian, Y., Chen, Z., Yu, Y., Shan, S., Rajput, V.D., Srivastava, S., Lin, D., 2022. Pyrolysis temperature affects the inhibitory mechanism of biochars on the mobility of extracellular antibiotic resistance genes in saturated porous media. J. Hazard. Mater. 439, 129668.

Forslund, A., Plauborg, F., Andersen, M.N., Markussen, B., Dalsgaard, A., 2011. Leaching of human pathogens in repacked soil lysimeters and contamination of potato tubers under subsurface drip irrigation in Denmark. Water Res. 45, 4367–4380.

Gargiulo, G., Bradford, S., Šimůnek, J., Ustohal, P., Vereecken, H., Klumpp, E., 2007. Bacteria transport and deposition under unsaturated conditions: The role of the matrix grain size and the bacteria surface protein. J. Contam. Hydrol. 92, 255–273.

Gee, G.W., Bauder, J.W., 1986. Particle size analysis. Nature http://dx.doi.org/10.1038/159717a0.

Grecco, K.L., de Miranda, J.H., Silveira, L.K., van Genuchten, M.T., 2019. HYDRUS-2D simulations of water and potassium movement in drip irrigated tropical soil container cultivated with sugarcane. Agric. Water Manag. 221, 334–347.

Guber, A.K., Shelton, D.R., Pachepsky, Y.A., 2005. Transport and retention of manure-borne coliforms in soil. Vadose Zo. J. 4, 828–837. http://dx.doi.org/10.2136/vzj2004.0097.

Guber, A.K., Shelton, D.R., Pachepsky, Y.A., Sadeghi, A.M., Sikora, L.J., 2006. Rainfall-induced release of fecal coliforms and other manure constituents: Comparison and modeling. Appl. Environ. Microbiol. 72, 7531–7539. http://dx.doi.org/10.1128/AEM.01121-06.

Guo, S., Liu, X., Zhao, H., Wang, L., Tang, J., 2021. High pyrolysis temperature biochar reduced the transport of petroleum degradation bacteria corynebacterium variabile HRJ4 in porous media. J. Environ. Sci. 100, 228–239.

Gurtler, J.B., Boateng, A.A., Han, Y., Douds, D.D., 2014. Inactivation of E. coli O157:H7 in cultivable soil by fast and slow pyrolysis-generated biochar. Foodborne Pathog. Dis. 11, 215–223. http://dx.doi.org/10.1089/fpd.2013.1631.
Hardie, M., Clothier, B., Bound, S., Oliver, G., Close, D., 2014. Does biochar influence soil physical properties and soil water availability? Plant Soil 376, 192–199.
Hassanizadeh, S.M., Schijven, J.F., 2000. Use of bacteriophages as tracers for the study of removal of viruses. In tracers and modelling in hydrogeology. In: Proceedings of TraM'2000, The International Conference on Tracers and Modelling in Hydrogeology. Liège, Belgium, May 2000, IAHS Press, pp. 167–174.
He, X., Xie, H., Gao, D., Rahman, K.U., Zhou, X., Wu, F., 2021. Biochar and intercropping with potato–onion enhanced the growth and yield advantages of tomato by regulating the soil properties, nutrient uptake, and soil microbial community. Front. Microbiol. 2334.
Herath, H.M.S.K., Camps-Arbestain, M., Hedley, M., 2013. Effect of biochar on soil physical properties in two contrasting soils: an Alfisol and an Andisol. Geoderma 188–197.
Honari, M., Ashrafzadeh, A., Khaledian, M., Vazifedoust, M., Mailhol, J.C., 2017. Comparison of HYDRUS-3D soil moisture simulations of subsurface drip irrigation with experimental observations in the South of France. J. Irrig. Drain. Eng. Am. Soc. Civ. Eng. 209–21143, 04017014.
Jeffery, S., Meinders, M.B., Stoof, C.R., Bezemer, T.M., van de Voorde, T.F., Mommer, L., van Groenigen, J.W., 2015. Biochar application does not improve the soil hydrological function of a sandy soil. Geoderma 251, 47–54.
Kaetzl, K., Lübken, M., Uzun, G., Gehring, T., Nettmann, E., Stenchly, K., Wichern, M., 2019. On-farm wastewater treatment using biochar from local agroresidues reduces pathogens from irrigation water for safer food production in developing countries. Sci. Total Environ. 682, 601–610.
Kameyama, K., Miyamoto, T., Shiono, T., Shinogi, T., 2012. Influence of sugarcane bagasse-derived biochar application on nitrate leachin in calcaric dark red soil. J. Environ. Qual. 41, 1131–1137.
Kandelous, M.M., Kamai, T., Vrugt, J.A., Šimůnek, J., Hanson, B., Hopmans, J.W., 2012. Evaluation of subsurface drip irrigation design and management parameters for alfalfa. Agric. Water Manag. 109, 81–93.
Kandelous, M.M., Šimůnek, J., 2010a. Comparison of numerical, analytical, and empirical models to estimate wetting patterns for surface and subsurface drip irrigation. Irrig. Sci. 28, 435–444. http://dx.doi.org/10.1007/s00271-009-0205-9.
Kandelous, M.M., Šimůnek, J., 2010b. Numerical simulations of water movement in a subsurface drip irrigation system under field and laboratory conditions using HYDRUS-2D. Agric. Water Manag. 97, 1070–1076. http://dx.doi.org/10.1016/j.agwat.2010.02.012.
Karandish, F., Simunek, J., 2016. A field-modeling study for assessing temporalvariations of soil–water-crop interactions under water-saving irrigationstrategies. Agric. Water Manag. 178, 291–303. http://dx.doi.org/10.1016/j.agwat.2016.10.009.
Klute, A., 1986. Water retention: laboratory methods. Methods Soil Anal. Part 1 Phys. Mineral. Methods 635–662.
Lehmann, J., Rillig, M.C., Thies, J., Masiello, C.A., Hockaday, W.C., Crowley, D., 2011. Biochar effects on soil biota - A review. Soil Biol. Biochem. 43, 1812–1836. http://dx.doi.org/10.1016/j.soilbio.2011.04.022.
Libutti, A., Francavilla, M., Monteleone, M., 2021. Hydrological properties of a clay loam soil as affected by biochar application in a pot experiment. Agronomy 11, 489.
Lim, T.J., Spokas, K.A., Feyereisen, G., Novak, J.M., 2016. Predicting the impact of biochar additions on soil hydraulic properties. Chemosphere 142, 136–144.
Madumathi, G., Philip, L., Bhallamudi, S.M., 2017. Transport of E. coli in saturated and unsaturated porous media: effect of physiological state and substrate availability. Sādhanā 42, 1007–1024. http://dx.doi.org/10.1007/s12046-017-0650-8.
Major, J., Rondon, M., Molina, D., Riha, S.J., Lehmann, J., 2012. Nutrient leaching in a Colombian savanna Oxisol amended with biochar. J. Environ. Qual. 41, 1076–1086.
Martin, D.L., Stegman, E.C., Freres, E., 1990. Irrigation scheduling principals. In: Hoffman, G.L., Howell, T.A., Solomon, K.H. (Eds.), Management of Farm Irrigation Systems. In: ASAE Monograph, pp. 155–372.
Mohanty, S., Boehm, A., 2014. Escherichia coli removal in biochar-augmented biofilter: effect of infiltration rate, initial bacterial concentration, biochar particle size, and presence of compost. Env. Sci Technol. 48, 11535–11542. http://dx.doi.org/10.1021/es5033162.
Mohanty, S.K., Cantrell, K.B., Nelson, K.L., Boehm, A.B., 2014. Efficacy of biochar to remove Escherichia coli from stormwater under steady and intermittent flow. Water Res. 61, 288–296.
Morales, I., Amador, J.A., Boving, T., 2015. Bacteria transport in a soil-based wastewater treatment system under simulated operational and climate change conditions. J. Environ. Qual. 44, 1459–1472.
Morales, I., Atoyan, J.A., Amador, J.A., Boving, T., 2014. Transport of pathogen surrogates in soil treatment units: Numerical modeling. Water 6, 818–838.
Mualem, Y., 1976. A new model for predicting the hydraulic conductivity of unsaturated porous media. Water Resour. Res. 12, 513–522.
Pang, L., McLeod, M., Aislabie, J., Šimůnek, J., Close, M., Hector, R., 2008. Modeling transport of microbes in ten undisturbed soils under effluent irrigation. Vadose Zo. J. 7, 97–111. http://dx.doi.org/10.2136/vzj2007.0108.
Perez-Mercadoa, L.F., Lalandera, C., Joelc, A., Ottosond, J., Dalahmeha, S., Vinnerås, B., 2019. Biochar filters as an on-farm treatment to reduce pathogens when irrigating with wastewater-polluted sources. J. Environ. Manag. 248, 109295.
Ponnusamy, V.K., Nagappan, S., Bhosale, R.R., Lay, C.H., Nguyen, D.D., Pugazhendhi, A., Woong, C.S., Kumar, G., 2020. Review on sustainable production of biochar through hydrothermal liquefaction: Physico-chemical properties and applications. Bioresour. Technol. 310, 123414.
Provenzano, G., 2007. Using HYDRUS-2D simulation model to evaluate wetted soil volume in subsurface drip irrigation systems. J. Irrig. Drain. Eng. 133, 342–349.
Pu, S., Li, G., Tang, G., Zhang, Y., Xu, W., Li, P., Feng, G., Ding, F., 2019. Effects of biochar on water movement characteristics in sandy soil under drip irrigation. J. Arid Land 11, 740–753.
Rabbi, S.M., Minasny, B., Salami, S.T., McBratney, A.B., Young, I.M., 2021. Greater, but not necessarily better: The influence of biochar on soil hydraulic properties. Eur. J. Soil Sci. 1–16.
Rayment, G.E., Higginson, F.R., 1992. Austarlian Laboratory Handbook of Soil and Water Chemical Methods. Inkata Press.
Rhoades, J.D., 1996. Salinity electrical conductivity and total dissolved solid. In: Page, A.L., Sommer, C.E., Nelson, P.W. (Eds.), Methods of Soil Analysis. In Part 3. Chemical Methods. ASA/SSSA Madison, Wisconsin, USA, pp. 417–436.
Rivera-Utrilla, J., Bautista-Toledo, I., Ferro-Garcia, M., Moreno-Castilla, C., 2001. Activated carbon surface modifications by adsorption of bacteria and their effect on aqueous lead adsorption. J. Chem. Technol. Biotechnol. 76, 1209–1215.
Sasidharan, S., Torkzaban, S., Bradford, S.A., Kookana, R., Page, D., Cook, P.G., 2016. Transport and retention of bacteria and viruses in biochar-amended sand. Sci. Total Environ. 548, 100–109.
Schijven, J.F., Šimůnek, J., 2002. Kinetic modeling of virus transport at the field scale. J. Contam. Hydrol. 55, 113–135.
Sepehrnia, N., Bachmann, J., Hajabbasi, M.A., Afyuni, M., Horn, M., 2018. Modeling transport of Escherichia coli and Rhodococcus erythropolis through wettable and repellent porous media. Colloids Surfaces B 172, 280–287.
Sepehrnia, N., Bachmann, J., Hajabbasi, M.A., Rezanezhad, F., Lichner, L., Hallett, P.D., Coyne, M., 2019. Transport, retention, and release of Escherichia coli and Rhodococcus erythropolis through dry natural soils as affected by water repellency. Sci. Total Environ. 694, 133666.
Šimůnek, J., Van Genuchten, M.T., Šejna, M., 2012. The HYDRUS software package for simulating the two-and three-dimensional movement of water, heat, and multiple solutes in variably-saturated porous media. In: Technical Manual.

Sims, J.T., 1996. Lime requirement. In: Page, A.L., Sommer, C.E., Nelson, P.W. (Eds.), Methods of Soil Analysis. In Part 3. Chemical Methods. ASA/SSSA. Madison, Wisconsin, USA, p. 491.
Skaggs, T.H., Trout, T.J., Rothfuss, Y., 2010. Drip irrigation water distribution patterns: effects of emitter rate, pulsing, and antecedent water. Soil Sci. Soc. Am. J. 74, 1886–1896.
Song, I., Stine, S.W., Choi, C.Y., Gerba, C.P., 2006. Comparison of crop contamination by microorganisms during subsurface drip and furrow irrigation. J. Environ. Eng. http://dx.doi.org/10.1061/(ASCE)0733-9372(2006)132:10(1243).
Staff, S.S., 2014. Keys to Soil Taxonomy, twelfth ed. US Department of Agriculture- NRCS, Washington, DC.
Suliman, W., Harsh, J.B., Fortuna, A.M., Garcia-Pérez, M., Abu-Lail, N.I., 2017. Quantitative effects of biochar oxidation and pyrolysis temperature on the transport of pathogenic and nonpathogenic Escherichia coli in biochar-amended sand columns. Environ. Sci. Technol. 51, 5071–5081.
Teshnizi, F.A., Ghobadinia, M., Abbasi, F., Hallett, P.D., Sepehrnia, N., 2023. Biochar and flow interruption control spatio-temporal dynamics of fecal coliform retention under subsurface drip irrigation. J. Contam. Hydrol. 253, 104128.
Thies, J.E., Rillig, M.C., 2012. Characteristics of biochar: biological properties. In: Biochar for Environmental Management. pp. 117–138.
Toková, L., Igaz, D., Horák, J., Aydin, E., 2020. Effect of biochar application and re-application on soil bulk density, porosity, saturated hydraulic conductivity, water content and soil water availability in a silty loam Haplic luvisol. Agronomy 10, 1005.
Valenca, R., Borthakur, A., Zu, Y., Matthiesen, E.A., Stenstrom, M.K., Mohanty, S.K., 2021. Biochar selection for Escherichia coli removal in stormwater biofilters. J. Environ. Eng. 147, 06020005.
van Genuchten, M.T., 1980. A closed-form equation for predicting the hydraulicconductivity of unsaturated soils. Soil Sci. Soc. Am. J. 44, 892–898.
Vieira, Y., dos Santos, J.M., Georgin, J., Oliveira, M.L., Pinto, D., Dotto, G.L., 2021. An overview of forest residues as promising low-cost adsorbents. Gondwana Res.
Wang, D., Li, C., Parikh, S.J., Scow, K.M., 2019. Impact of biochar on water retention of two agricultural soils – A multi-scale analysis. Geoderma 340, 185–191. http://dx.doi.org/10.1016/j.geoderma.2019.01.012.
Wen, J., Li, J., Wang, Z., Li, Y., 2017. Modelling water flow and escherichia coli transport in unsaturated soils under drip irrigation. Irrig. Drain. 66, 738–749. http://dx.doi.org/10.1002/ird.2142.
Willmott, C.J., 1982. Some comments on the evaluation of model performance. Bull. Am. Meteorol. Soc. 63, 1309–1313.
Wu, Y., Yang, A., Zhao, Y., Liu, Z., 2019. Simulation of soil water movement under biochar application based on the HYDRUS-1D in the black soil region of China. Appl. Ecol. Environ. Res. 17, 4183–4192.
Xi, B., Bloomberg, M., Watt, M.S., Wang, Y., Jia, L., 2016. Modeling growth response to soil water availability simulated by HYDRUS for a mature triploid populus tomentosa plantation located on the North China Plain. Agric. Water Manag. 176, 243–254. http://dx.doi.org/10.1016/j.agwat.2016.06.017.
Yin, D., Li, H., Wang, H., Guo, X., Wang, Z., Lv, Y., Ding, G., Jin, L., Lan, Y., 2021. Impact of different biochars on microbial community structure in the Rhizospheric soil of rice grown in Albic soil. Molecules 26, 4783.
Zhong, H., Liu, G., Jiang, Y., Yang, J., Liu, Y., Yang, X., Liu, Z., Zeng, G., 2017. Transport of bacteria in porous media and its enhancement by surfactants for bioaugmentation: a review. Biotechnol. Adv. 35, 490–504.
Zhu, X., Chen, B., Zhu, L., Xing, B., 2017. Effects and mechanisms of biochar-microbe interactions in soil improvement and pollution remediation: A review. Environ. Pollut. 227, 98–115. http://dx.doi.org/10.1016/j.envpol.2017.04.032.